Inorganic Chemistry
Article

Inorg. Chem. **2010**, *49*, 397–406 **397**
DOI: 10.1021/ic9009898

Efficient and Long-Time Stable Red Iridium(III) Complexes for Organic Light-Emitting Diodes Based on Quinoxaline Ligands

Daniel Schneidenbach,[†] Sven Ammermann,[†] Marc Debeaux,[†] Andreas Freund,[†] Mike Zöllner,[†] Constantin Daniliuc,[†,‡] Peter G. Jones,[†,‡] Wolfgang Kowalsky,[†] and Hans-Hermann Johannes*[,†]

[†]*Labor für Elektrooptik, Institut für Hochfrequenztechnik and* [‡]*Institut für Anorganische Chemie, Technische Universität Braunschweig, Bienroder Weg 94, D-38106 Braunschweig, Germany*

Received May 20, 2009

We report the design and characterization of three heteroleptic orange-red phosphorescent iridium(III) complexes bearing two 2-(4-fluorophenyl)-3-methyl-quinoxaline (fpmqx) cyclometalated ligands combined with three different ancillary ligands, triazolylpyridine (trz), picolinate (pic), and acetylacetonate (acac). All of these complexes emit an orange to red color in the spectral range of 605−628 nm in dichloromethane. Strong spin−orbit coupling of the iridium atom allows the formally forbidden mixing of singlet and triplet states. Because of the structureless phosphorescent line shapes and low Stokes shifts between triplet metal-to-ligand charge-transfer (^{3}MLCT) absorption and phosphorescent emission, we propose that emission originates predominantly from the ^{3}MLCT state with a lesser admixture of totally ligand-based $^3(\pi-\pi^*)$ states. The influence of 5d-electron densities of the iridium center on highest occupied molecular orbitals leads to high emission quantum yields in toluene (Φ_p = 0.39−0.42) and to short triplet lifetimes. Cyclovoltammetry measurements show reversible oxidation peaks from 0.74 to 0.92 V and reversible reduction waves with potentials ranging from −1.58 to −2.05 V versus Cp_2Fe/Cp_2Fe^+. All complexes have been applied in simple test devices and also in stable, long-living devices to evaluate their electroluminescent device performances, for which we especially report the influence of the chosen ancillary ligands on emission colors, efficiencies, and device lifetimes. We obtained narrowband emission ranging from 613 to 630 nm with a full width at half-maximum of 64−71 nm, and a maximum in power efficiency of η_p = 14.6 lm/W at a current density of J = 0.01 mA/cm^2 for [(fpmqx)$_2$Ir(pic)]. The operating lifetimes of [(fpmqx)$_2$Ir(trz)] in both neat and mixed matrixes were longer than that of the established stable tris(1-phenylisoquinolinato)iridium(III) [Ir(piq)$_3$]. From the lifetime measurements, it becomes clear that the stability is strongly correlated to the type of ancillary ligand. An extrapolated lifetime of 58 000 h with an initial brightness of 1000 cd/m^2, together with a very low voltage increase of 0.2 V over a time period of 1000 h (starting voltage of 4.1 V), was achieved. Such a high device lifetime is attributed to the chemical stability of all materials toward both charge carriers and excitons.

Introduction

Recent progress has been achieved in research on organometallic complexes containing third-row transition-metal ions, especially Ir^{3+}, with respect to their use for future organic light-emitting diode (OLED) applications.[1] High efficiency, chemical stability, and well-defined emission characteristics of organometallic phosphors are the most important requirements. A large number of octahedral neutral 5d^6 complexes, containing iridium as a metal center and heteroleptic (C^N) cyclometalated ligands, have been extensively studied for multiple emission colors by the group of Thompson.[1] Strong spin−orbit coupling, originating from the heavy metal iridium atom, allows fast energy transfer from singlet to triplet states and also removes the forbidden character of radiative transition to ground states. In the case of fluorescent emitters, only 25% of internal quantum efficiency (IQE) can be obtained, caused by spin statistics. Hence, applying a triplet emitter can theoretically result in 100% IQE.[2] Nearly 100% IQE for photoluminescence (PL) in the solid state has been demonstrated for green and blue emission using *fac*-tris(2-phenylpyridinato)iridium(III) [*fac*-Ir(ppy)$_3$] and bis(4,6-difluorophenyl)pyridinato-*N*,*C*^{2})iridium(picolinate) [FIrpic].

*To whom correspondence should be addressed. Phone: + 49 531 391 − 8002/+ 49 531 391 − 2006. Fax: +49 531 391 − 8004. E-mail: h2.johannes@ihf.tu-bs.de.

(1) (a) Baldo, M. A.; O'Brien, D. F.; You, Y.; Shoustikov, A.; Sibley, S.; Thompson, M. E.; Forrest, S. R. *Nature* **1998**, *395*, 151. (b) Baldo, M. A.; Thompson, M. E.; Forrest, S. R. *Nature* **2000**, *403*, 750. (c) Baldo, M. A.; Lamansky, S.; Burrows, P. E.; Thompson, M. E.; Forrest, S. R. *Appl. Phys. Lett.* **1999**, *75*, 4–6. (d) Lamansky, S.; Djurovich, P.; Murphy, D.; Razzaq, F. A.; Lee, H. E.; Adachi, C.; Burrows, P. E.; Forrest, S. R.; Thompson, M. E. *J. Am. Chem. Soc.* **2001**, *123*, 4304–4312.

(2) (a) Kawamura, Y.; Gouchi, K.; Brooks, J.; Brown, J. J.; Sasabe, H.; Adachi, C. *Appl. Phys. Lett.* **2005**, *86*, 071104. (b) Adachi, C.; Baldo, M. A.; Thompson, M. E.; Forrest, S. R. *J. Appl. Phys.* **2001**, *90*, 5048–5051.

Published on Web 12/18/2009

Compared to green and blue phosphorescent iridium complexes, orange- to red-emitting iridium complexes tend to be more limited in quantum yields.[2] Nonradiative rates (k_{nr}) increase, while radiative rates (k_r) decrease for longer wavelength emission, according to the energy gap law. This is attributable to increasing vibrational overlap between excited and ground states.[3] The synthesis of new promising orange−red iridium complexes is generally based on the design of rigid cyclometalated ligands with a low degree of freedom for vibrational loss. In the past few years, promising phosphorescent orange−red iridium complexes for OLEDs have been investigated.[4−6] Nitrogen-containing heterocycles such as quinolines/isoquinolines,[4] quinazolines,[5] and quinoxalines[6] have been of special interest in accomplishing orange to red phosphorescent emission. High external quantum efficiencies and ultrastable phosphorescent pure red devices have been demonstrated using [Ir(piq)$_3$] as a triplet emitter in adapted and stable *pin*-OLED architectures.[7] With the realization of high efficiencies and excellent colors throughout the visible spectrum, the phosphorescent OLED luminance lifetime is the key for commercial success. The origin of intrinsic luminance loss and voltage increase in OLEDs has been intensively investigated in recent studies. It is widely accepted that intrinsic degradation has a chemical (electrochemical) basis. Through bond cleavage, fragments are generated, which can react in further radical addition reactions.[8] The resulting products act as nonradiative recombination centers, luminescence quenchers, and deep charge traps. There is a large deficit of information about the operating/chemical stability of earlier reported OLED materials concerning both charge transport and emitter materials.[9]

In 2004 and 2005, various groups presented a new iridium complex for deep red emission, bis(2,3-diphenylquinoxaline)iridium(III) acetylacetonate [(dpqx)$_2$Ir(acac)], which exhibits a maximum emission peak at around 670 nm in solution and around 680 nm in resulting devices, showing a high quantum yield.[10] Because of this resulting deep red emission of [(dpqx)$_2$Ir(acac)], it was necessary to tune the emission to the orange−red region to improve luminance efficiency. Luminescence taking place in octahedral iridium complexes generally involves electronic transitions from excited states, which are a mixture of metal-to-ligand charge transfer ^{3}(MLCT) and various ligand-based $^3(\pi-\pi^*)$ states, to ground states. Changing electron densities in the extended π systems of ligands directly affects the electronic transitions in the resulting complexes. Various researchers have changed the emission characteristics by substitution, using electron-withdrawing atoms such as fluorine but keeping the "symmetric" diphenylquinoxaline basic system because of its synthetic benefits.[11]

In this paper, we demonstrate efficient and long-living phosphorescent iridium complexes based on the new "asymmetric" cyclometalated ligand 2-(4-fluorophenyl)-3-methylquinoxaline (fpmqx) in combination with three different ancillary ligands, triazolylpyridine (trz), picolinate (pic), and acetylacetonate (acac). By using (fpmqx) cyclometalated ligands, we achieved a further hypsochromic shift in both photoluminescence and electroluminescence (EL) compared to "symmetric" quinoxaline ligands. The ancillary ligands employed in this study are established in the literature, and their influence on the emission properties is well-known.[1d,12] Herein, we show that the influence of the ancillary ligands can be important for achieving long device lifetimes in addition to their affect on emission colors. Information in the literature about device degradation mechanisms and the influence of the employed iridium complexes is very limited, and a deeper understanding has not yet been achieved. Such information may help in future materials development for realizing stable OLED materials.

Experimetal Section

General Information. Air- and moisture-sensitive reactions were carried out under nitrogen in flame-dried flasks using standard Schlenk techniques. Organic reagents and dry solvents stored over a molecular sieve were obtained from Sigma-Aldrich, Acros Organics, Fluka, and Chempur and were used as delivered. The reaction progress was monitored by thin-layer chromatography on Polygram SIL G/UV_254 plates (Macherey-Nagel). Silica Gel 60 M (Macherey-Nagel) was used for column chromatographic separations. ^{1}H and ^{13}C NMR spectra were recorded at 298 K on Bruker DPX-400 and Bruker AV2-600 spectrometers in $CDCl_3$ and DMSO-d_6 operating at 400 and 600 MHz, respectively. ^{1}H chemical shifts are given in parts per million referenced to TMS as an internal standard for $CDCl_3$ and to residual protons of DMSO-d_6 at 2.50 ppm. ^{13}C shifts are given relative to $CDCl_3$ at 77.0 ppm and DMSO-d_6 at 39.4 ppm. Elemental analyses were performed on a Vario EL Elemental Analysis Instrument (Elementar Co.). Mass spectra were run on a Thermofinnigan MAT95 (EI (electron impact) at 70 eV) and a Thermofinnigan MAT95XLT (ESI (electrospray ionization) with an applied voltage of 1.3−1.8 kV). UV−vis measurements were carried out on a Varian Cary 100 Bio spectrophotometer in dichloromethane solution.

Spectroscopic and CV Measurements. PL and EL spectra were measured on a Kontron SF-25 (PL) and a Tec5 MMS UV−vis (EL) spectrophotometer. Quantum efficiency measurements were carried out at room temperature in a degassed toluene solution. Before measurement, the solution was degassed by at least four freeze−pump−thaw cycles. A solution of *fac*-Ir(ppy)$_3$ in degassed toluene (Φ_p = 0.40) was used as a reference.[13]

(3) Cummings, S. D.; Eisenberg, R. *J. Am. Chem. Soc.* **1996**, *118*, 1949–1960.

(4) (a) Tsuboyama, A.; Iwawaki, H.; Furugori, M.; Mukaide, T.; Kamatani, J.; Igawa, S.; Moriyama, T.; Miura, S.; Takiguchi, T.; Okada, S.; Hoshino, M.; Ueno, K. *J. Am. Chem. Soc.* **2003**, *125*, 12971–12979. (b) Yang, C. H.; Tai, C.-C.; Sun, I.-W. *J. Mater. Chem.* **2004**, *14*, 947–950. (c) Li, C.-L.; Su, Y.-J.; Tao, Y.-T.; Chou, P.-T.; Chien, C.-H.; Cheng, C.-C.; Liu, R.-S. *Adv. Funct. Mater.* **2005**, *15*(3), 387–395. (d) Fang, K.-H.; Wu, L.-L.; Huan, Y.-T.; Yang, C.-H.; Sun, I.-W. *Inorg. Chim. Acta* **2006**, *359*, 441–450.

(5) Song, Y.-H.; Yeh, S.-J.; Chen, C.-T.; Chi, Y.; Liu, C.-S.; Yu, J.-K.; Hu, Y.-H.; Chou, P.-T.; Peng, S.-M.; Lee, G.-H. *Adv. Funct. Mater.* **2004**, *14*(12), 1221–1226.

(6) Duan, J. P.; Sun, P. P.; Cheng, C. H. *Adv. Mater.* **2004**, *15*(3), 224–228.

(7) Meerheim, R.; Walzer, K.; Pfeiffer, M.; Leo, K. *Appl. Phys. Lett.* **2006**, *89*, 061111.

(8) (a) Kondakov, D. Y.; Lenhart, W. C.; Nichols, W. F. *J. Appl. Phys.* **2007**, *101*, 024512. (b) Kondakov, D. Y. *J. Appl. Phys.* **2008**, *104*, 084520.

(9) (a) Giebink, N. C.; D'Andrade, B. W.; Weaver, M. S.; Mackenzie, P. B.; Brown, J. J.; Thompson, M. E.; Forrest, S. R. *J. Appl. Phys.* **2008**, *103*, 044509. (b) Scholz, S.; Corten, C.; Walzer, K.; Kuckling, D.; Leo, K. *Org. Electron.* **2007**, *8*, 709–717.

(10) (a) Zhang, G. L.; Liu, Z. H.; Guo, H. Q. *Chin. Chem. Lett.* **2004**, *15*, 1349–1352. (b) Fujii, H.; Sakurai, H.; Tani, K.; Wakisaka, K.; Hirao, T. *IEICE Electron. Express* **2005**, *2*, 260–266. (c) Gao, J; You, H.; Fang, J; Ma, D; Wang, L.; Jing, X.; Wang, F. *Synth. Met.* **2005**, *155*, 168–171.

(11) (a) Hwang, F.-M.; Chen, H.-Y.; Chen, P.-S.; Liu, C.-S.; Chi, Y.; Shu, C.-F.; Wu, F.-I.; Chou, P.-T.; Peng, S.-M.; Lee, G.-H. *Inorg. Chem.* **2005**, *44*, 1344–1353. (b) Ha, Y.; Seo, J.-H.; Kim, Y. K. *Synth. Met.* **2008**, *158*, 548–552. (c) Tani, K.; Fujii, H.; Mao, L.; Sakurai, H.; Hirao, T. *Bull. Chem. Soc. Jpn.* **2007**, *80*, 783–788.

(12) (a) Chou, P.-T.; Chi, Y *Chem.—Eur. J.* **2007**, *13*, 380–395. (b) Coppo, P.; Plummer, E. A.; De Cola, L. *Chem. Commun.* **2004**, 1774–1775.

(13) Brooks, J.; Babayan, Y.; Lamasky, S.; Djurovich, P. I.; Tsyba, I.; Bau, R.; Thompson, M. E. *Inorg. Chem.* **2002**, *41*, 3055–3066.

Measurements of triplet lifetimes (solution and solid state) were performed using a streak camera (Hamamatsu C 4334) using excitation with a short laser pulse (third harmonic Nd:YVO_4) at 355 nm with a repetition rate of 2 kHz and a pulse width of approximately 700 ps. Solution measurements were performed in degassed and N_2-saturated toluene using $Ir(piq)_3$ as a reference. For solid-state measurements, the iridium complexes were coevaporated with matrix material 4,4′,4″-tris(carbazole-9-yl)-triphenylamine (TCTA) on a Si wafer at a doping concentration of 8 vol %. The wafers were measured in a special gadget, flushed with a constant flow of nitrogen to avoid molecular oxygen quenching.

Cyclic voltammetry (CV) and differential pulse voltammetry (DPV) were performed using a Metrohm μAutolab Type III apparatus equipped with a 1 mm platinum disk working electrode, a platinum wire counter electrode, and a saturated Ag/AgCl reference electrode, in anhydrous CH_2Cl_2 (CV) and anhydrous DMF (DPV) containing 0.1 M Bu_4NPF_6 as a supporting electrolyte. The analyte concentration was set to 0.1 mM. The potentials were measured against a Ag/Ag^+ reference electrode with a ferrocene reference standard using a scan rate of 100 mV s^{-1}.

Device Fabrication. OLED devices were fabricated by high vacuum thermal evaporation (10^{-8} mbar) on a precleaned indium tin oxide (ITO)-coated glass substrate with a sheet resistance of 14 Ω sq^{-1}. The thickness of the organic layers was controlled by quartz crystal monitors, and the deposition rate was regulated to 0.03−0.4 Å s^{-1}. The L−I−V characteristics of the OLEDs were measured under ambient conditions using a source measure unit (Keithley 2400) and a calibrated Si photodiode (Advantest TQ 8221).

The simple test architecture consisted of 20 nm of *N*,*N*′-di(naphthalene-1-yl)-*N*,*N*′-diphenyl-benzidine (α-NPD), 20 nm of 8 vol % iridium complexes **1**−**3** doped in 4,4′,4″-tris-(carbazole-9-yl)-triphenylamine (TCTA), 45 nm of 1,3,5-tris-(1-phenyl-1*H*-benzimidazole-2-yl)benzene (TPBi), and a LiF/Al cathode.

The stable lifetime architecture consisted of a molybdenum-(VI) oxide (MoO_3) p-doped α-NPD layer, neat α-NPD, and α-NPD or a mixed matrix system consisting of α-NPD and bis-(2-methyl-8-quinolato)-4-(phenyl-phenolato)-aluminum(III) (BAlq) as host materials (volume ratios 1:1 and 1:3 vol %) doped by the red emitters (**1**−**3** and $[Ir(piq)_3]$; 15 vol %), BAlq, 4,7-diphenyl-1,10-phenanthroline (BPhen) n-doped with Cs_2CO_3, and an Al cathode.

The devices were encapsulated using a glass lid encapsulation. The device lifetime was measured in a commercial OLED lifetime test system (Botest) using a substrate with an active area of 20 mm^2. All lifetime tests were carried out at room temperature over a time period of 1000 h with an initial brightness of 1000 cd/m^2. α-NPD, TCTA, TPBi, BAlq, and BPhen were received from Sensient; $[Ir(piq)_3]$ was received from American Dye Source Inc. (all in sublimed form). All new iridium complexes were chemically purified and dried in an ultra-high vacuum prior to use.

X-Ray Structure Determinations. The data for **1** were collected on a Bruker SMART 1000 CCD diffractometer; data for **2** on an Oxford Diffraction Xcalibur S diffractometer, both using monochromated Mo Kα radiation. Absorption corrections were based on multiscans. The structures were refined anisotropically on F^2 using the program SHELXL-97.[14] Hydrogen atoms were included using rigid methyl groups or a riding model. *Special features of refinement are as follows:* The structure of **1** contains a severely disordered chloroform site that could not be refined satisfactorily. Accordingly, the program SQUEEZE (A. L. Spek, University of Utrecht, Netherlands) was used to remove mathematically the effects of the solvent. For calculations of formula mass and so forth, a solvent content of one chloroform per asymmetric unit was assumed. For **2**, both solvent molecules are well-ordered; the methanol OH hydrogen was refined freely.

Preparation of Ligands. 2,4-Pentanedione and picolinic acid were purchased from Acros Organics and Fluka. 2-(5-Phenyl-4*H*-1,2,4-triazol-3-yl)pyridine was prepared as described by Case.[15]

The cyclometalated ligand (fpmqx)H was prepared starting from 4-fluoropropiophenone. The "asymmetric" dione was synthesized using the procedure of Danswan et al.[16] The characterization data of this dione are in good agreement with those of other workers, who used α,β-epoxyketones or 1,3-dioles as starting materials.[17] A further condensation reaction from the diole and 1,2-diaminobenzene results in a high yield of the cyclometalated quinoxaline ligand (fpmqx)H. Iridium complexes containing 2-(4-fluorophenyl)-3-methylquinoxaline were unknown until now.

Synthesis of 1-(4-Fluorophenyl)propane-1,2-dione (fppd). To a mixture of 4-fluoropropiophenone (4.0 g, 26.3 mmol) and aluminum chloride (52 mg, 0.4 mmol) in 20 mL of dry diethyl ether, bromine (3.2 mL, 63.1 mmol) was added dropwise at 0 °C over 10 min. The red−brown suspension was heated to reflux with stirring for 21 h under nitrogen. After cooling to room temperature, the solvent was removed under reduced pressure. The oil thus obtained was added to a solution of sodium methoxide (3.83 g, 71.0 mmol) in 30 mL of dry methanol at 0 °C over 15 min. Following the addition of 8.2 mL of concentrated hydrochloric acid, the mixture was warmed slowly to room temperature and stirred for 1.5 h. The precipitate was filtered off and washed repeatedly with diethyl ether. The combined filtrate was concentrated and extracted with chloroform (3 × 100 mL). The combined organic phases were dried with anhydrous magnesium sulfate; the solvent was removed under reduced pressure and the crude product purified by flash chromatography (eluent: hexane/ethylacetate = 10:1, R_f = 0.29). A yellow oil was obtained (2.61 g).

Spectral data are as follows. Yield: 60%. MS (GC/MS, EI): *m*/*z* 166 (5) [M^+], 123 (100), 95 (44), 75 (17). ^{1}H NMR (400.1 MHz, $CDCl_3$): δ 8.12−8.05 (AA′XX′, *N* = 9.0 Hz, $J_{H,F}$ = 5.5 Hz, 2H), 7.20−7.14 (AA′XX′, *N* = 9.0 Hz, $J_{H,F}$ = 8.4 Hz, 2H), 2.53 (s, 3H, CH_3). ^{13}C NMR (100.6 MHz, $CDCl_3$): δ 200.09 (s), 189.24 (s), 166.63 (s, $J_{C,F}$ = 257.8 Hz), 133.25 (d, $J_{C,F}$ = 9.7 Hz), 128.26 (s, $J_{C,F}$ = 2.9 Hz), 116.13 (d, $J_{C,F}$ = 22.0 Hz), 26.25 (q, CH_3). ^{19}F NMR (376.5 MHz, $CDCl_3$): δ −102.31 (s, $J_{F,C}$ = 257.7 Hz, 1F).

Synthesis of 2-(4-Fluorophenyl)-3-methylquinoxaline (fpmqx)-H. To a solution of 1-(4-fluorophenyl)propane-1,2-dione (2.44 g, 14.7 mmol) and 1,2-diaminobenzene (1.91 g, 17.6 mmol) in 15 mL of acetonitrile was added iodine (0.37 g, 1.5 mmol). The reaction mixture was stirred for 10 min at room temperature. The solvent was removed under reduced pressure, and the crude product was purified by flash chromatography (eluent: hexane/ethyl acetate = 5:1, R_f = 0.29) to give a yellow solid (3.37 g).

Spectral data are as follows. Yield: 96%. MS (EI): *m*/*z* 238 (64) [M^+], 237 (100), 197 (18), 117 (16). ^{1}H NMR (400.1 MHz, $CDCl_3$): δ 8.12−8.08 (m, 1H), 8.08−8.03 (m, 1H), 7.74 (m_c, 1H), 7.72 (m_c, 1H), 7.69−7.62 (AA′XX′, *N* = 8.8 Hz, $J_{H,F}$ = 5.3 Hz, 2H), 7.28−7.18 (AA′XX′, *N* = 8.8 Hz, $J_{H,F}$ = 8.7 Hz, 2H), 2.78 (s, 3H, CH_3). ^{13}C NMR (100.6 MHz, $CDCl_3$): δ 163.24 (s, $J_{C,F}$ = 249.1 Hz), 153.80 (s), 152.29 (s), 141.25 (s), 140.95 (s), 135.09 (s, $J_{C,F}$ = 3.4 Hz), 130.94 (d, $J_{C,F}$ = 8.4 Hz), 129.83 (d), 129.33 (d), 129.15 (d), 128.33 (d), 115.62 (d, $J_{C,F}$ = 21.7 Hz), 24.36 (q, CH_3).

(14) Sheldrick, G. M. *Acta Crystallogr.* **2008**, *A64*, 112–122.

(15) Case, F. H. *J. Org. Chem.* **1965**, *30*, 931–933. (b) Case, F. H. *J. Heterocycl. Chem.* **1970**, *7*, 1001–1005.

(16) Danswan, G.; Kennewell, P. D.; Tully, W. R. *J. Heterocycl. Chem.* **1989**, *26*, 293–299.

(17) (a) Yadav, Y. S.; Biswas, S. K.; Srinivas, R. *Synthesis* **2006**, *24*, 4237–4241. (b) Chang, C.-L.; Kumar, M. P.; Liu, R. S. *J. Org. Chem.* **2004**, *69*, 2793–2796.

Scheme 1. Synthesis[a]

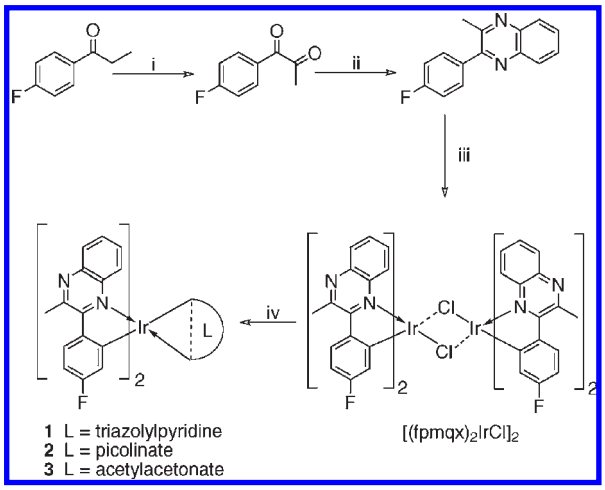

[a] (i) $AlCl_3$, Br, Et_2O; MeONa, MeOH; (ii) 1,2-diaminobenzene, I_2, MeCN; (iii) $IrCl_3$, ethoxyethanol, H_2O; (iv) ligand, CH_2Cl_2/EtOH − 3:1, *t*BuONa.

^{19}F NMR (376.5 MHz, $CDCl_3$): δ −112.56 (s, $J_{F,C}$ = 249.1 Hz, 1F). Anal. Calcd for $C_{15}H_{11}F_2N_2$: C, 75.62; H, 4.65; N, 11.76. Found: C, 75.32; H, 4.63; N, 11.42.

Synthesis of (2-(4-Fluorophenyl)-3-methylquinoxaline)-iridium(III)-μ-chloro Complex ([(fpmqx)$_2$IrCl]$_2$). 2-(4-Fluorophenyl)-3-methylquinoxaline (1.86 g, 7.8 mmol) and iridium(III) chloride hydrate (1.14 g, 3.8 mmol) were suspended in a degassed solution of 30 mL of 2-ethoxyethanol and 10 mL of distilled water and heated to reflux for 46 h under nitrogen. After cooling to room temperature, the suspension was filtered. The residue was washed with water and hexane and dried under a vacuum. A dark red solid was obtained (1.86 g). The μ-chloro-bridged dimer product was used without further purification.

Spectral data are as follows. Yield: 67%. MS (ESI, acetonitrile/toluene = 1:1): *m*/*z* 667 (100). ^{1}H NMR (600.1 MHz, DMSO-d_6): δ 8.93 ("d", br, $J_{H,H}$ = 8.7 Hz, 4H), 8.27 (dd, $J_{H,H}$ = 9.0 Hz, $J_{H,F}$ = 5.8 Hz, 4H), 8.10 (dd, $J_{H,H}$ = 8.2, 1.4 Hz, 4H), 7.81 (ddd, $J_{H,H}$ = 8.2, 6.8, 1.3 Hz, 4H), 7.68 (ddd, $J_{H,H}$ = 8.7, 6.8, 1.4 Hz, 4H), 6.84 ("dt", $J_{H,H}$ = 9.0, 2.7 Hz, $J_{H,F}$ = 8.9 Hz, 4H), 6.03 (dd, $J_{H,F}$ = 9.5 Hz, $J_{H,H}$ = 2.7 Hz, 4H), 3.27 (s, 12H, CH_3). ^{13}C NMR (150.9 MHz, DMSO-d_6): δ 163.32 (s), 161.17 (s, $J_{C,F}$ = 253.9 Hz), 160.33 (s), 151.54 (s), 142.13 (s, $J_{C,F}$ = 1.2 Hz), 140.55 (s), 139.79 (s), 131.90 (d, $J_{C,F}$ = 9.7 Hz), 129.56 (d), 129.50 (d), 127.77 (d), 127.72 (d), 120.51 (d, $J_{C,F}$ = 17.4 Hz), 108.74 (d, $J_{C,F}$ = 22.3 Hz), 26.77 (q, *C*H$_3$). ^{19}F NMR (376.5 MHz, DMSO-d_6): δ −109.76 (s, 4F). Anal. Calcd for $C_{60}H_{40}Cl_2F_4Ir_2N_8$: C, 51.32; H, 2.87; N, 7.98; Cl, 5.05. Found: C, 50.85; H, 2.93; N, 7.59; Cl, 5.25.

Preperation of Complexes 1−3. All cyclometalated iridium(III) complexes were prepared using the following procedure given as an illustrative example for complex **1**. Starting from the μ-chloro-bridged dimer [(fpmqx)$_2$IrCl]$_2$, the complexes **2** and **3** are synthesized by exchanging 2-(5-phenyl-4*H*-1,2,4-triazol-3-yl)pyridine with picolinic acid and 2,4-pentanedione.

Synthesis of *mer*-Bis(2-(6-fluoro-3-methylquinoxaline-2-yl-κN^1)phenyl-κC^2)(3-phenyl-5-(2-pyridyl-κN)-1,2,4-triazol-1-yl)iridium(III) (1). The mixture of μ-chloro-bridged dimer [(fpmqx)$_2$IrCl]$_2$ (0.80 g, 0.57 mmol), 2-(5-phenyl-4*H*-1,2,4-triazol-3-yl)pyridine (0.32 g, 1.42 mmol), and potassium *tert*-butoxide (0.16 g, 1.42 mmol) in 20 mL of dry dichloromethane and 6 mL of dry ethanol was stirred at room temperature for 20 h under nitrogen (see Scheme 1). The solvent was removed under reduced pressure and the crude product purified by flash chromatography (eluent: dichloromethane/acetone = 20:1, R_f = 0.38). A red solid was obtained (0.81 g).

Spectral Data for [*mer*-(fpmqx)$_2$Ir(trz)] (1). Yield: 80%. MS (EI): *m*/*z* 888 (100) [M$^+$], 667 (35). ^{1}H NMR (600.1 MHz, $CDCl_3$): δ 8.42 (dd, $J_{H,H}$ = 8.9 Hz, $J_{H,F}$ = 5.4 Hz, 1H), 8.28 (dd, $J_{H,H}$ = 9.0 Hz, $J_{H,F}$ = 5.5 Hz, 1H), 8.05 ("d", $J_{H,H}$ = 8.9 Hz, 1H), 7.98−7.92 (m, 3H), 7.81 (dd, $J_{H,H}$ = 8.2, 1.3 Hz, 1H), 7.78 (dd, $J_{H,H}$ = 8.2, 1.0 Hz, 1H), 7.77 (d, br, $J_{H,H}$ = 7.8 Hz, 1H), 7.62 (dt, $J_{H,H}$ = 7.8, 7.8, 1.3 Hz, 1H), 7.44 (ddd, $J_{H,H}$ = 8.2, 6.9, 1.1 Hz, 1H), 7.36 (ddd, $J_{H,H}$ = 8.2, 7.1, 1.0 Hz, 1H), 7.36−7.31 (m, 2H), 7.29−7.25 (m, 1H), 7.22 ("d", $J_{H,H}$ = 8.6 Hz, 1H), 7.13 (m$_c$, $J_{H,H}$ = 6.9, 1.3 Hz, 1H), 7.12 (m$_c$, 1H), 6.96 (dt, $J_{H,H}$ = 8.9, 2.7 Hz, $J_{H,F}$ = 8.7 Hz, 1H), 6.91−6.86 (m, 2H), 6.60 (dd, $J_{H,F}$ = 9.0 Hz, $J_{H,H}$ = 2.7 Hz, 1H), 6.13 (dd, $J_{H,F}$ = 9.2 Hz, $J_{H,H}$ = 2.6 Hz, 1H), 3.34 (s, 3H, CH_3), 3.34 (s, 3H, CH_3). ^{13}C NMR (150.9 MHz, $CDCl_3$): δ 165.34 (s), 164.64 (s), 163.27 (s), 163.10 (s, $J_{C,F}$ = 258.2 Hz), 162.76 (s, $J_{C,F}$ = 6.1 Hz), 162.45 (s, $J_{C,F}$ = 256.1 Hz), 162.32 (s), 154.08 (s, $J_{C,F}$ = 7.3 Hz), 151.93 (s), 151.60 (s), 150.76 (s), 146.06 (d), 142.31 (s, $J_{C,F}$ = 1.4 Hz), 141.72 (s, $J_{C,F}$ = 1.3 Hz), 140.63 (s), 139.89 (s), 139.66 (s), 139.58 (s), 138.49 (d), 132.94 (s), 131.94 (d, $J_{C,F}$ = 9.4 Hz), 131.10 (d, $J_{C,F}$ = 9.6 Hz), 130.91 (d), 129.95 (d), 129.01 (d), 128.97 (d), 128.71 (d), 128.19 (d), 127.85 (d), 127.76 (d), 126.97 (d), 125.97 (d), 124.05 (d), 123.59 (d), 122.89 (d, $J_{C,F}$ = 16.9 Hz), 121.02 (d), 120.76 (d, $J_{C,F}$ = 17.8 Hz), 110.05 (d, $J_{C,F}$ = 23.9 Hz), 109.89 (d, $J_{C,F}$ = 23.5 Hz), 27.40 (q, *C*H$_3$), 26.82 (q, *C*H$_3$). ^{19}F NMR (376.5 MHz, $CDCl_3$): δ −108.54 (s, 1F), −109.54 (s, 1F). Anal. Calcd for $C_{43}H_{29}F_2IrN_8$: C, 58.16; H, 3.29; N, 12.62. Found: C, 58.01; H, 3.36; N, 12.23.

Spectral Data for [*mer*-(fpmqx)$_2$Ir(pic)] (2). Yield: 96%. MS (EI): *m*/*z* 789 (100) [M$^+$], 745 (48), 744 (58), 667 (90), 507 (35), 237 (87). ^{1}H NMR (400.1 MHz, $CDCl_3$): δ 8.52 (dd, $J_{H,H}$ = 8.7, 1.3 Hz, 1H), 8.40 (dd, $J_{H,H}$ = 9.1 Hz, $J_{H,F}$ = 5.6 Hz, 1H), 8.23 (dd, $J_{H,H}$ = 9.0 Hz, $J_{H,F}$ = 5.5 Hz, 1H), 7.97 (dd, $J_{H,H}$ = 8.3, 1.3 Hz, 1H), 7.92 (ddd, $J_{H,H}$ = 5.4, 1.5, 0.7 Hz, 1H), 7.91 (dd, $J_{H,H}$ = 8.2, 1.6 Hz, 1H), 7.78 (ddd, $J_{H,H}$ = 7.8, 1.5, 0.7 Hz, 1H), 7.67 ("dt", $J_{H,H}$ = 7.8, 7.5, 1.5 Hz, 1H), 7.61 (ddd, $J_{H,H}$ = 8.2, 6.9, 1.3 Hz, 1H), 7.55 (ddd, $J_{H,H}$ = 8.7, 6.9, 1.6 Hz, 1H), 7.44 (ddd, $J_{H,H}$ = 8.3, 6.9, 1.2 Hz, 1H), 7.35 (ddd, $J_{H,H}$ = 7.5, 5.4, 1.5 Hz, 1H), 7.19 (dd, $J_{H,H}$ = 8.7, 1.2 Hz, 1H), 6.92 (ddd, $J_{H,H}$ = 9.1, 2.7 Hz, $J_{H,F}$ = 8.5 Hz, 1H), 6.91 (ddd, $J_{H,H}$ = 8.7, 6.9, 1.3 Hz, 1H), 6.77 ("dt", $J_{H,H}$ = 9.0, 2.7 Hz, $J_{H,F}$ = 8.8 Hz, 1H), 6.54 (dd, $J_{H,F}$ = 9.3 Hz, $J_{H,H}$ = 2.7 Hz, 1H), 5.91 (dd, $J_{H,F}$ = 9.2 Hz, $J_{H,H}$ = 2.7 Hz, 1H), 3.33 (s, 3H, CH_3), 3.32 (s, 3H, CH_3). ^{13}C NMR (100.6 MHz, $CDCl_3$): δ 171.25 (s), 164.08 (s), 162.76 (s, $J_{C,F}$ = 258.5 Hz), 162.57 (s, $J_{C,F}$ = 257.1 Hz), 162.24 (s), 156.53 (s, $J_{C,F}$ = 7.3 Hz), 154.52 (s, $J_{C,F}$ = 7.0 Hz), 152.20 (s), 151.96 (s), 150.70 (s), 145.44 (d), 141.90 (s, $J_{C,F}$ = 1.8 Hz), 140.81 (s, $J_{C,F}$ = 1.6 Hz), 140.58 (s), 140.47 (s), 140.24 (s), 139.93 (s), 138.44 (d), 131.90 (d, $J_{C,F}$ = 9.7 Hz), 131.46 (d, $J_{C,F}$ = 10.7 Hz), 131.41 (d), 130.14 (d), 129.56 (d), 129.17 (d), 128.72 (d), 128.09 (d), 127.67 (d), 126.54 (d), 123.91 (d), 122.73 (d, $J_{C,F}$ = 17.5 Hz), 121.02 (d, $J_{C,F}$ = 17.7 Hz), 110.12 (d, $J_{C,F}$ = 23.1 Hz), 109.71 (d, $J_{C,F}$ = 23.1 Hz), 27.47 (q, *C*H$_3$), 27.41 (q, *C*H$_3$). ^{19}F NMR (376.5 MHz, $CDCl_3$): δ −108.27 (s, $J_{F,C}$ = 258.3 Hz, 1F), −109.23 (s, $J_{F,C}$ = 257.1 Hz, 1F). Anal. Calcd for $C_{36}H_{24}F_2IrN_5O_2$: C, 54.81; H, 3.07; N, 8.88. Found: C, 54.61; H, 3.01; N, 9.00.

Spectral Data for [*mer*-(fpmqx)$_2$Ir(acac)] (3). Yield: 82%. MS (EI) *m*/*z* 766 (27) [M$^+$], 667 (100); ^{1}H NMR (400.1 MHz, $CDCl_3$) δ 8.15 (dd, $J_{H,H}$ = 9.0 Hz, $J_{H,F}$ = 5.6 Hz, 2H), 8.09 (dd, $J_{H,H}$ = 8.7, 1.2 Hz, 2H), 7.95 (dd, $J_{H,H}$ = 8.2, 1.4 Hz, 2H), 7.57 (ddd, $J_{H,H}$ = 8.2, 6.9, 1.2 Hz, 2H), 7.35 (ddd, $J_{H,H}$ = 8.7, 6.9, 1.4 Hz, 2H), 6.69 ("dt", $J_{H,H}$ = 9.0, 2.7 Hz, $J_{H,F}$ = 8.8 Hz, 2H), 6.08 (dd, $J_{H,F}$ = 9.3 Hz, $J_{H,H}$ = 2.7 Hz, 2H), 4.48 (s, 1H), 3.26 (s, 6H, CH_3), 1.40 (s, 6H, CH_3); ^{13}C NMR (100.6 MHz, $CDCl_3$) δ 185.84 (s), 163.64 (s), 162.00 (s, $J_{C,F}$ = 256.1 Hz), 156.44 (s, $J_{C,F}$ = 7.1 Hz), 151.22 (s), 141.97 (s, $J_{C,F}$ = 1.7 Hz), 141.31 (s), 139.79 (s), 131.23 (d, $J_{C,F}$ = 9.6 Hz), 129.92 (d), 129.12 (d), 128.21 (d), 125.52 (d), 122.49 (d, $J_{C,F}$ = 17.2 Hz), 109.25 (d, $J_{C,F}$ = 23.3 Hz), 100.02 (d), 28.10 (q, *C*H$_3$), 27.16 (q, *C*H$_3$); ^{19}F NMR (376.5 MHz, $CDCl_3$) δ −110.49 (s, $J_{F,C}$ = 256.4 Hz, 2F);

Scheme 2. Iridium Complexes **1**−**3**

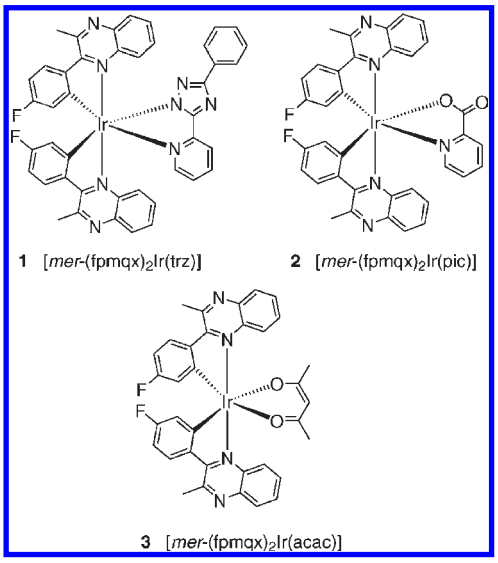

Anal. Calcd for $C_{35}H_{27}F_2IrN_4O_2$: C, 54.89; H, 3.55; N, 7.32; Found: C, 54.61; H, 3.57; N, 7.34.

Results and Discussion

Synthesis of the Complexes. Complexes **1**−**3** depicted in Scheme 2 were obtained in very high yields from the quinoxaline ligands by a conventional two-step synthesis. The μ-chloro-bridged dimer was formed by the reaction of the cyclometalated ligand precursor with $IrCl_3 \cdot H_2O$ in a mixture of 2-ethoxyethanol and water.[18] The monomeric complexes were obtained by the treatment of the dimer with the ancillary ligand precursors in the presence of potassium *tert*-butoxide.[12b] The resulting complexes are air-stable, sublimable, and sufficiently soluble for photophysical and electrochemical measurements. The complexes can easily be processed in ultra-high vacuum processes. These compounds were characterized by NMR, mass spectra, elemental analysis, and in the case of **1** and **2** X-ray diffraction.

Crystal Structures. In both complexes, the coordination geometry at iridium is distorted octahedral. The main distortions are associated with the differing trans influences of the ligands (e.g., Ir−N trans to C is lengthened) and with the restricted bites of the chelating ligands (bite angles ca. 80°). However, it is clear that the molecules also suffer from steric crowding. Compound **1** (Figure 1, left) has short intramolecular contacts such as H7···C35 (2.68) and H29···H30A (2.05 Å), although the contact H22···N6 (2.38 Å) may be regarded as an intramolecular hydrogen bond. The Ir atom is significantly displaced out of the chelation planes of the fmpqx ligands (by 0.32 Å for the system N1/C10 and 0.36 Å for N3/C25) but is coplanar with the trz chelation plane (mean deviation of 5 atoms, 0.04 Å). In the fmpqx ligands, the atoms C1 and C16 lie slightly out of the planes of the other nine atoms of the respective bicyclic system (by 0.18, 0.13 Å); the C_6H_4 ring is rotated by 19 and 14° with respect to the best plane of the C_4N_2 ring. In the trz ligand, the central ring subtends interplanar angles of 14° to the ring C31−35,N5 and 8° to the ring C38−43. The crowding and associated distortion in compound **2** (Figure 2) seems slightly more severe, although the general features are similar to those of **1**. The Ir atom lies 0.46 and 0.38 Å out of the chelating planes of N1/C10 and N3/C25, respectively, but lies in the chelating plane of the pic ligand (mean deviation 0.02 Å). There is a short intramolecular contact H7···C35 of 2.54 Å. The corresponding deviations of C1 and C16 are 0.23 and 0.14 Å, and the interplanar angles are 21° and 18°. The solvent molecules of **2** are well-ordered and participate in hydrogen-bonding systems (Figure 2). The methanol OH group is the donor of a classical H bond to O2, and both of these O atoms are acceptors for C−H···O hydrogen bonds from the dichloromethane molecule. The short intramolecular contact H22···O1 may also be regarded as a favorable interaction. Crystallographic data for **1**·$CHCl_3$ and **2**·CH_2Cl_2·MeOH are given in Table 1.

Photophysical Data. The UV−vis absorption and luminescence spectra of complexes **1**−**3** in dichloromethane are given, together with the absorption spectrum of the free quinoxaline ligand, in Figure 3. The absorption bands of all complexes show very similar absorption characteristics and are slightly shifted from each other at a longer wavelength. The extinction coefficients for $^1(\pi-\pi^*)$-ligand-based (17 000−65 300 M^{-1} cm^{-1}) and metal-to-ligand charge-transfer absorption bands (600−6900 M^{-1} cm^{-1}) are in the expected range.[1d] Short wavelength absorptions of these complexes, seen in the former two absorption bands below 400 nm, are mostly ligand-based $^1(\pi-\pi^*)$ absorptions, showing similar shapes to those of the free quinoxaline ligand. Both singlet MLCT (^{1}MLCT) and triplet MLCT (^{3}MLCT) absorption bands are observed in iridium-centered complexes at a longer wavelength and are shown enlarged in Figure 3b. Low-energy, spin-allowed ^{1}MLCT ← S_0 absorptions with very weak shoulders at 540−550 nm show typically low extinction coefficients (1400−1600 M^{-1} cm^{-1}) close to those of spin-forbidden ^{3}MLCT absorptions (600−700 M^{-1} cm^{-1}). Strong spin−orbit coupling leads to direct, strongly allowed ^{3}MLCT ← S_0 transitions with weak shoulders at 580−590 nm. Thus, strong admixing of singlet and triplet states results in low triplet lifetimes (τ_p solution/ 1.7−2.6 μs) in combination with high emission quantum yields (Φ_p/0.39−0.42). The triplet lifetime of the reference [Ir(piq)$_3$] was measured as τ_p = 1.2 μs, which is in good agreement with earlier work.[19] High radiative rate constants (k_r), which are crucial factors for limiting triple−triplet annihilation in devices, prohibit fast efficiency roll-off for high current densities. Furthermore, it has been proposed that increasing the radiative rate directly affects operating device lifetimes.[9a] All three iridium complexes show a strong phosphorescence emission at 605 nm (**1**), 606 nm (**2**), and 628 nm (**3**) in dichloromethane with an appropriate full width at half-maximum (fwhm) of 73, 72, and 73 nm, respectively. The line shapes of the phosphorescence spectra are broad and structureless with no vibronic fine structure. The iridium complexes **1**−**3** exhibit a small Stokes shift between ^{3}MLCT absorption and phosphorescent emission with values of 27 (**1**), 26 (**2**), and 36 nm (**3**), respectively. The

(18) Sprouse, S.; King, K. A.; Spellane, P. J.; Watts, R. J. *J. Am. Chem. Soc.* **1984**, *106*, 6647–6653.

(19) Reinecke, S.; Walzer, K.; Leo, K. *Phys. Rev. B* **2007**, *75*, 125328.

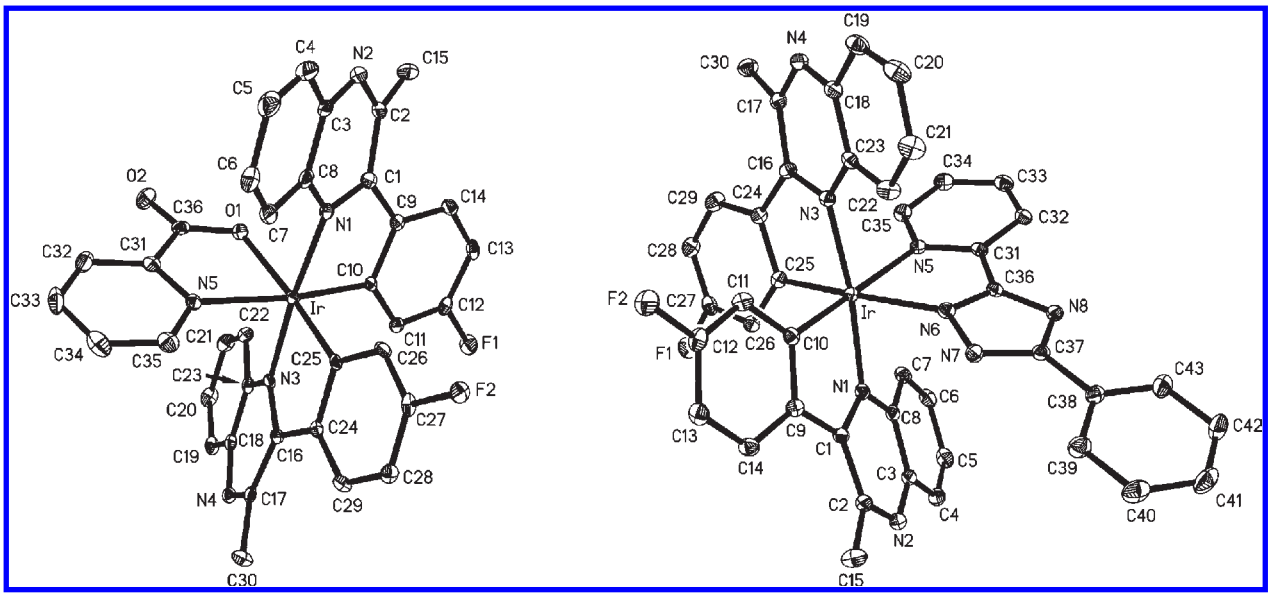

Figure 1. (Left) The molecule of **1** in the crystal. Ellipsoids correspond to 50% probability levels. H atoms are omitted for clarity. Bond lengths and angles at Ir (Å, deg): Ir−N1, 2.075(2); Ir−N3, 2.059(2); Ir−N5, 2.213(2); Ir−N6, 2.147(2); Ir−C10, 1.992(3); Ir−C25, 1.980(3); C10−Ir−N1, 78.9(1); C25−Ir−N3, 79.6(1); N1−Ir−N6, 80.9(1). (Right) The molecule of **2** in the crystal. Ellipsoids correspond to 30% probability levels. H atoms and solvent are omitted for clarity. Bond lengths and angles at Ir (Å, deg): Ir−N1, 2.062(3); Ir−N3, 2.057(2); Ir−N5, 2.170(3); Ir−O1, 2.156(2); Ir−C10, 1.985(3); Ir−C25, 1.971(3); C10−Ir−N1, 79.8(1); C25−Ir−N3, 79.9(1); O1−Ir−N5, 76.0(1).

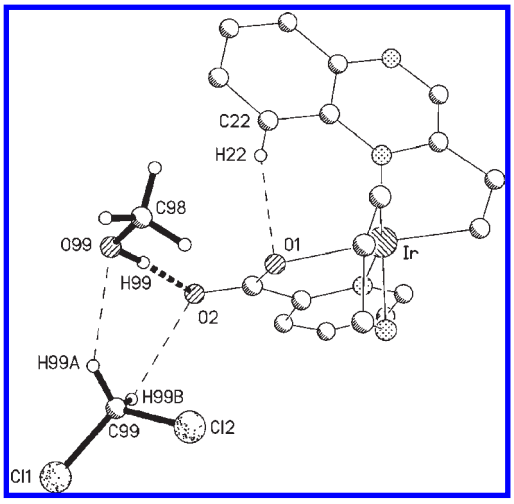

Figure 2. H-bonding interactions in $2\cdot CH_2Cl_2\cdot MeOH$. Parts of the molecule of **2** are omitted for clarity. Relevant distances (Å): H22···O1, 2.18; H99···O2, 1.96; H99A···O99, 2.35; H99B···O2, 2.54.

complex bis(2-phenylpyridinato)iridium(III) (acetylacetonate) $[(ppy)_2Ir(acac)]$ exhibits a small Stokes shift between the absorption and emission bands, while (2-(2′-benzothienyl)-pyridinato)iridium(acetylacetonate) $[(btp)_2Ir(acac)]$ gives a rather large shift. The emissive states of these two complexes have been reported to have predominantly ^{3}MLCT $[(ppy)_2Ir(acac)]$ and $^3(\pi-\pi^*)$ $[(btp)_2Ir(acac)]$ character.[1d,20] We propose that the triplet emission of the iridium complexes **1**−**3** originates predominantly from a ^{3}MLCT state with a lesser admixture of totally ligand-based $^3(\pi-\pi^*)$ states. Photophysical properties of complexes **1**−**3** are given in Table 2.

(20) (a) Lee, Y. H.; Kim, Y. S. *Curr. Appl. Phys.* **2007**, *7*, 504–508. (b) Colombo, M. G.; Brunold, C.; Riedener, T.; Güdel, H. U.; Förtsch, M.; Bürgi, H.-B. *Inorg. Chem.* **1994**, *33*, 545–550.

Table 1. Crystallographic Data for $1\cdot CHCl_3$ and $2\cdot CH_2Cl_2\cdot MeOH$

	$1\cdot CHCl_3$	$2\cdot CH_2Cl_2\cdot MeOH$
formula	$C_{44}H_{30}Cl_3F_2IrN_8$	$C_{38}H_{30}Cl_2F_2IrN_5O_3$
fw	1007.31	905.77
T (K)	133	100
λ (Å)	0.71073	0.71073
cryst habit/size(mm)	red prism, 0.23 × 0.15 × 0.13	red prism, 0.3 × 0.06 × 0.06
cryst syst	monoclinic	monoclinic
space group	$P2_1/c$	$P2_1/n$
a (Å)	12.7240(5)	10.4887(6)
b (Å)	16.2591(7)	8.2755(3)
c (Å)	18.6472(8)	39.004(2)
β (deg)	99.572(1)	94.325(6)
V (Å^3)	3809.4(3)	3375.9(3)
Z	4	4
ρ_{calcd} (Mg m^{-3})	1.756	1.782
μ (mm^{-1})	3.77	4.17
2θ(max)	61	55
no. reflns	80440	73795
unique reflns/R(int)	11638/0.051	7750/0.056
no. params	489	467
R1 ($I > 2\sigma(I)$)	0.0290	0.0292
wR2 (all reflns)	0.0659	0.0509
S	1.04	1.09
$\Delta\rho$ (e Å^{-3})	1.47	1.09

Using "asymmetric" 2-(4-fluorophenyl)-3-methylquinoxaline as a cyclometallating ligand in iridium complexes results in a further hypsochromic shift compared to "symmetric" 2,3-bis(4-fluorophenyl) quinoxaline. The achieved hypsochromic shift can be explained by substitution of the phenyl ring with a methyl fragment. Compared to "symmetric" diphenylquinoxaline ligands, the π conjugation in the novel "asymmetric" quinoxaline-based moieties cannot be extended into the absent phenyl ring. The resulting elongated π system is smaller for the "asymmetric" iridium complexes **1**−**3**.

Electrochemical Data. The electrochemical properties of these iridium complexes were investigated by cyclic

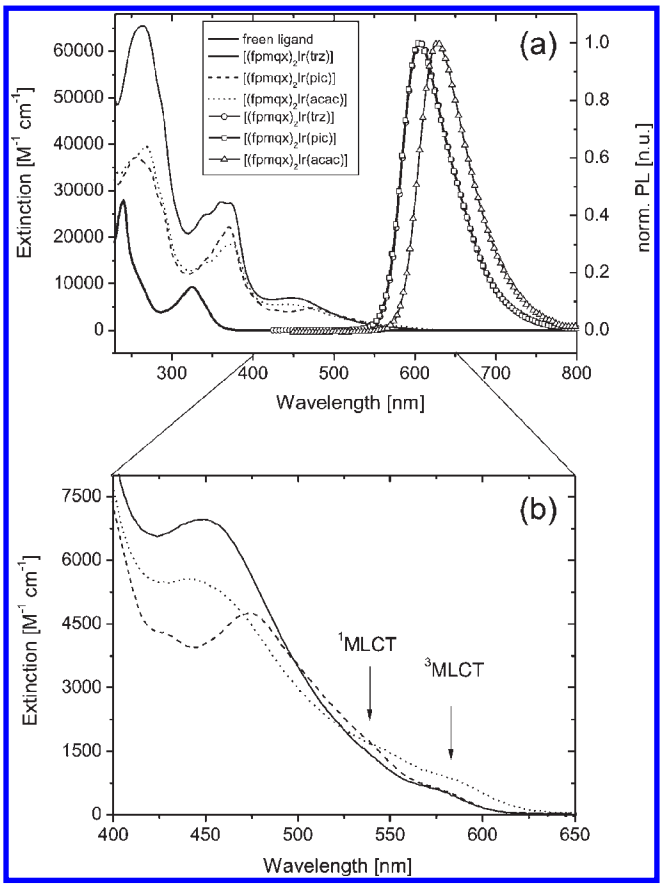

Figure 3. (a) UV−vis absorption (CH_2Cl_2) and PL-emission (CH_2Cl_2) spectrum of complexes **1**−**3**. (b) Zoom-in UV−vis absorption spectrum in the range 400−650 nm.

voltammetry (CV/CH_2Cl_2) and differential pulse voltammetry (DPV/DMF) using ferrocene as a reference standard ($Cp_2Fe/Cp_2Fe^+ = 0.45$ V in DMF). CV curves are displayed in Figure 4 for **1** (a), **2** (b), and **3** (c). The electrochemical data determined by DPV are given in Table 3. All complexes **1**−**3** exhibit reversible one-electron oxidation at high positive potentials in the region of 0.74−0.92 V, indicating typical low-lying HOMO energies for quinoxaline complexes.[11] The oxidation peaks are further shifted to higher potentials with an increase in π-accepting character of the ancillary ligands (E^{ox}: triazole 0.92 > picolinate 0.87 > acetylacetonate 0.74). In a cathodic sweep, all complexes show two reversible reduction waves with potentials ranging from −1.58 to −2.05 V. As seen for the oxidation potentials, the different π-withdrawing character of various ancillary ligands also causes the first reduction potentials to be less negative (E^{red1}: triazole −1.58 > picolinate −1.63 > acetylacetonate −1.72). Bandgap (ΔE_{opt}) values of 2.04 eV for complexes **1** and **2** and 1.97 eV for complex **3**, calculated from absorption onset, λ_{abs}^{onset}, belong to the first triplet excited state energies (T_1) of these complexes.

As reported in earlier electrochemical and theoretical studies, the first oxidation of iridium (C^N) heterocyclic complexes occurs mainly at the iridium center together with a minor contribution from the cyclometalated, carbanion-containing phenyl fragment.[21] Using time-dependent density functional theory for highly efficient iridium complexes, the electron densities of the highest occupied molecular orbitals (HOMOs) have been calculated to be localized up to 50% at the iridium center. Compared to other 2-phenylpyridyl iridium complexes, the first oxidation potentials of the complexes **1**−**3** are affected by the electron-withdrawing character of the fluorine substituent. This leads to low-lying HOMO and lowest unoccupied molecular orbital (LUMO) energies. Substitution with fluorine at the 4 and 6 positions has a much larger effect on HOMOs and LUMOs than substitution at the 3 and 5 positions, as known from earlier studies.[22] The reduction occurs primarily at the electron-poor heterocyclic portion of the (C^N) cyclometalated ligand. LUMOs have been calculated to be mainly localized on the neutral heterocyclic part of the ligands, with negligible iridium 5d character. The heterocyclic quinoxaline part of the ligand defines the LUMO energies, the bandgap, and thus the emission color.

Electroluminescent Devices. Basic electroluminescent properties of all three complexes have been demonstrated using a simple test-device architecture. α-NPD was used for hole-transport; TPBi was used for electron-transport and further acts as a hole-blocking material. Such a hole-blocking layer is needed to keep the recombination zone inside the emission layer.[23] The iridium complexes **1**−**3** were doped in a suitably wide bandgap matrix consisting of TCTA. We chose TCTA because of its suitable HOMO energy to realize good hole injection properties.[24] It is known that carbazole derivatives such as TCTA and 4,4′-bis(*N*-carbazolyl)biphenyl (CBP) are not chemically stable, so they cannot be used for long-living OLEDs.[8b,9] The current efficiencies of devices **I**−**III** are shown in Figure 5, and the EL spectra of all three complexes **1**−**3** in devices **I**−**III** match those trends of the same compounds in solution and are shown in Figure 6. Thus, all EL emissions originate from the triplet excited state. For **1** and **2**, very narrow-band EL characteristics peaked at 613 and 615 nm with Commission International de L'Eclairage (CIE) 1931 chromaticity coordinates of (0.64, 0.35). Complex **3** shows a deeper red emission peaked at 630 nm with CIE chromaticity coordinates of (0.68, 0.32). All devices show low turn-on voltages and high maximum brightness with values of 2.9 V, 21 528 cd/m^2 at 12 V for device **I**; 2.5 V, 28 019 cd/m^2 at 12.6 V for device **II**; and 2.4 V, 13 252 cd/m^2 at 12 V for device **III**.

Table 4 summarizes EL characteristics and performance data of devices **I**−**III**. Device **II** shows the highest device efficiencies. We obtained a maximum in power efficiency of $\eta_p = 14.6$ lm/W and a maximum in external quantum efficiency of $\eta_{ext} = 12\%$ for orange−red emission in device **II**, which is in the same range as $Ir(piq)_3$ in regard to η_{ext}.[7] For pure red emission in device **III**, we achieved a maximum in power efficiency of $\eta_p = 5.7$ lm/W

(21) (a) Hay, J. H. *J. Phys. Chem. A* **2002**, *106*, 1634–1641. (b) Lee, Y. H.; Kim, Y. S. *Thin Solid Films* **2007**, *515*, 5079–5083. (c) Tamayo, A. B.; Alleyne, B. D.; Djurovich, P. I.; Lamansky, S.; Tsyba, I.; Ho, N. N.; Bau, R.; Thompson, M. E. *J. Am. Chem. Soc.* **2003**, *125*, 7377–7387.

(22) (a) D'Andrade, B. W.; Datta, S.; Forrest, S. R.; Djurovich, P.; Polikarpov, E.; Thompson, M. E. *Org. Electronics* **2005**, *6*, 11–20. (b) Xu, M.; Zhou, R.; Wang, G.; Yu, J. *Inorg. Chim. Acta* **2009**, *362*, 2183–2188.

(23) Li, Y.; Fung, M. K.; Xie, Z.; Lee, s.-T.; Hung, L.-S.; Shi, J. *Adv. Mater.* **2002**, *14*, 1317–1321.

(24) Meyer, J.; Hamwi, S.; Bülow, T.; Johannes, H.-H.; Riedl, T.; Kowalsky, W. *Appl. Phys. Lett.* **2007**, *91*, 113506.

Table 2. Photophysical Properties of Complexes **1**−**3**

	λ_{abs}^{max}/nm (ε, M^{-1} cm^{-1})[a]	λ_{max} [nm][a]	Φ_p[b]	τ_p [μs][c]
1	263 (65300), 342 (24900), 361 (27500), 372 (27200), 449 (br, 6900), 539 (sh, 1400), 578 (sh, 600)	605	0.42	2.6 (0.99)
2	256 (37200), 370 (22300), 474 (br, 4700), 542 (sh, 1600), 580 (sh, 600)	606	0.39	2.1 (0.90)
3	255 (sh, 38200), 269 (39400), 346 (sh, 17000), 371 (19000), 457 (br, 5600), 547 (sh, 1500), 592 (sh, 700)	628	0.41	1.7 (0.53)

[a] Measured in CH_2Cl_2; concentrantion ~2×10^{-5} M. [b] Quantum yield in degassed toluene referenced to $\Phi_p = 0.40$ [*fac*-Ir(ppy)$_3$]. [c] Measured in degassed and N_2-saturated toluene, $\tau_p = 1.2$ μs [Ir(piq)$_3$];[19] fit, mono exponential.

Table 3. Electrochemical Properties of Complexes **1**−**3**

complex	E^{ox} [V][a]	E^{red} [V][a]	HOMO [eV][b]	$LUMO_{opt}$ [eV][c]	λ_{abs}^{onset} [nm]	ΔE_{opt} [eV][c]	ΔE_{DPV} [eV][d]
1	0.92	−1.58, −1.94	−5.72	−3.68	607	2.04	2.50
2	0.87	−1.63, −1.90	−5.67	−3.63	609	2.04	2.50
3	0.74	−1.72, −2.05	−5.54	−3.57	624	1.97	2.47

[a] Potential values from DPV measurements versus Cp_2Fe/Cp_2Fe^+. [b] Deduced from equation HOMO = −4.8 eV − E^{ox}. [c] Calculated from optical edge λ_{abs}^{onset} using equation $LUMO_{opt}$ = HOMO + ΔE_{opt}. [d] Band gap DPV using equation $E^{ox} - E^{red1}$.

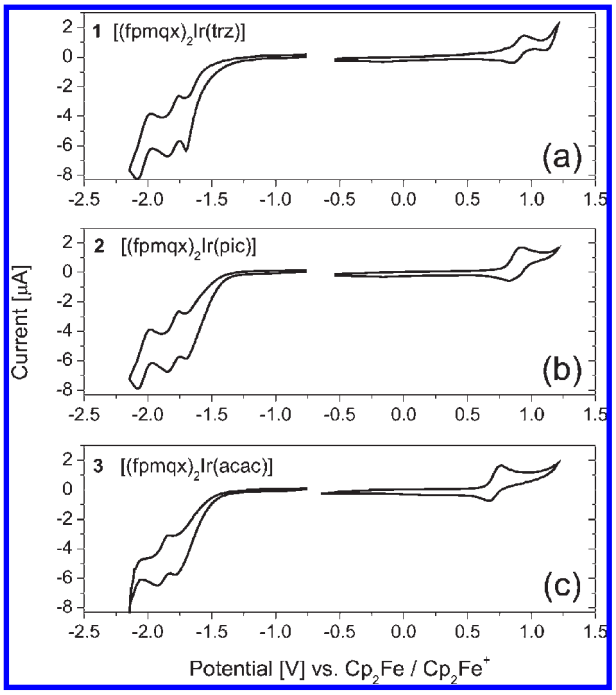

Figure 4. Cyclic voltammograms of **1** (a), **2** (b), and **3** (c) versus Cp_2Fe/Cp_2Fe^+.

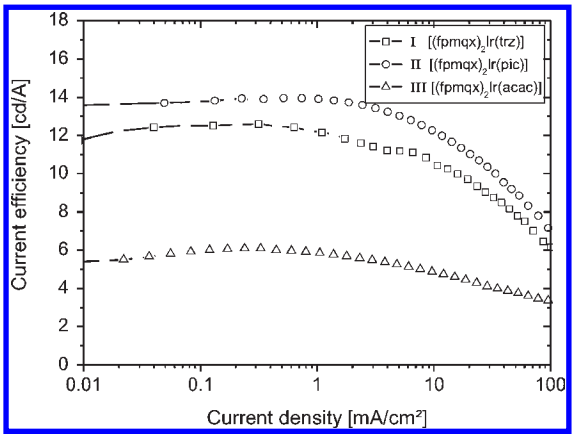

Figure 5. Current efficiencies of devices **I**−**III**.

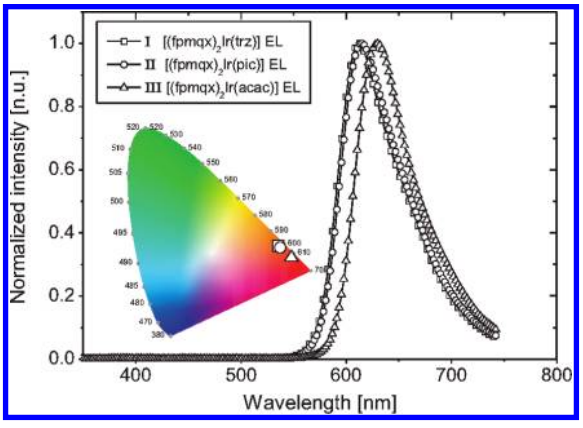

Figure 6. EL spectra and CIE coordinates of devices **I**−**III** at 30 mA/cm^2.

and a maximum in external quantum efficiency of approximately 8%. For all three devices, η_I versus current density is given in Figure 6. A limited roll-off over a wide range of current densities can be easily seen. This indicates a fast optical depopulation of triplet states, high intersystem crossing rates, and little influence of quenching processes as anticipated from photophysical experiments.[25] Quenching processes are mainly attributable to a longer phosphorescence lifetime, τ_p, of triplet emitting states in comparison with the lifetime, τ_f, of singlet emitting states, which are in the range of nanoseconds. Further, such a limited roll-off in quantum efficiencies can only be achieved when the host−guest energy transfer of the matrix and emitter is highly efficient.

Operating Lifetime Performance. As reported before, the chemical stability, including electrochemical and photochemical stabilities, of all employed materials is the crucial factor for long-living OLEDs. We chose a stable *pin*-OLED device setup similar to the reported [Ir(piq)$_3$] OLED presented by Meerheim et al.[7] Unlike these devices, we used a MoO_3 p-doped α-NPD layer as the hole injection layer, whose operating stability has also been proven in several studies.[26] With these *pin*-OLED

(25) Adachi, C.; Baldo, M. A.; Forrest, S. R.; Lamansky, S.; Thompson, M. E.; Kwong, R. C. *Appl. Phys. Lett.* **2001**, *78*, 1622–1624.

(26) (a) Jiang, X.-Y.; Zhang, Z.-L.; Cao, J.; Khan, M. A.; Haq, K.-u.; Zhu, W. Q. *J. Phys. D. Appl. Phys.* **2007**, *40*, 5553–5557. (b) Shin, W.-J.; Lee, J.-Y.; Kim, J. C.; Yoon, T.-H.; Kim, T.-S.; Son, O.-K. *Org. Electron.* **2008**, *9*, 333–338.

Table 4. Characteristics of Simple Test-Device OLEDs **I**−**III**

device	λ_{max} [nm]	CIE *X*	CIE *Y*	fwhm [nm]	max brightness [cd/m^2] at V	turn-on voltage [V]	η_P [lm/W] / η_I[cd/A] (η_{ext}) [%] at *J* [mA/cm^2] 0.01	1	10	100
I	613	0.64	0.35	70	21528 (12.0)	2.9	11.1/11.9 [9.6]	8.9/12 [9.8]	5.6/10.5 [8.5]	2.2/6.4 [5.1]
II	615	0.64	0.35	71	28019 (12.6)	2.5	14.6/13.4 [11.5]	10.4/13.9 [12]	6.4/12.3 [10.5]	2.6/6.9 [5.5]
III	630	0.68	0.32	64	13252 (12.0)	2.4	5.7/5.4 [7.2]	3.5/5.9 [7.8]	2.1/4.8 [6.4]	1.0/3.2 [3.9]

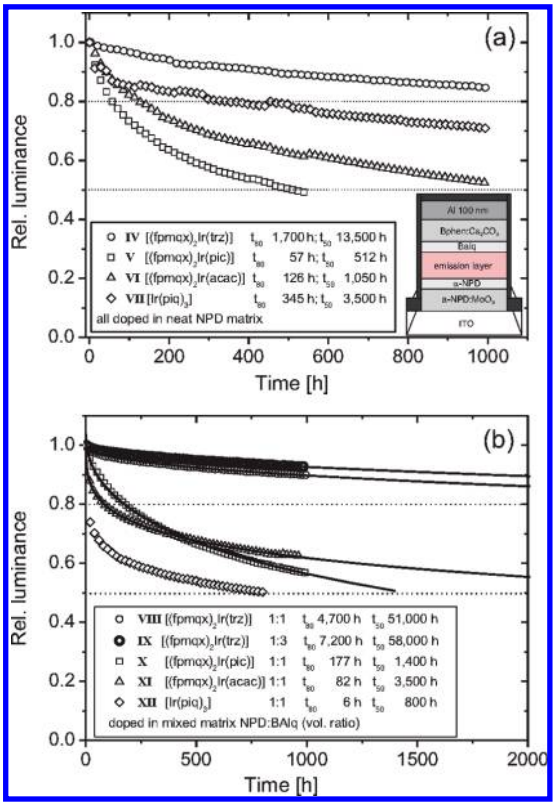

Figure 7. Lifetime performance of all novel iridium complexes **1**−**3** compared to [Ir(piq)$_3$], all tested at an initial brightness of 1000 cd/m^2. (a) Emitters doped in a neat α-NPD matrix (devices **IV**−**VII**); inset: t_{80}, t_{50} lifetimes, device architecture. (b) Emitters doped in a mixed matrix consisting of α-NPD and BAlq (devices **VIII**−**XII**); [(fpmqx)$_2$Ir(trz)] was also tested with different mixed matrix ratios (NPD/BAlq, 1:1 and 1:3); inset: t_{80}, t_{50} lifetimes; extrapolation using the SED function.[27]

structures, we achieved turn-on voltages below 2 V and operating voltages between 3.5 and 4.1 V (1000 cd/m^2) for all devices. [Ir(piq)$_3$] is the most stable red phosphorescent emitter reported in the literature so far and thus is helpful in evaluating the lifetime performance of new iridium complexes.

All devices were tested under the same conditions for a time period of 1000 h with an initial brightness of 1000 cd/m^2 (room temperature). We determined and extrapolated the time for the luminance decrease to 80% (t_{80}) and 50% (t_{50}) of initial brightness. In the first device setups (shown in Figure 7, **IV**−**VII**), neat α-NPD, a hole transporting material, was chosen as the matrix material. Hence, we expect the recombination and emission zone to be strongly located at the hole blocking layer of BAlq. We also expect to find an imbalance of holes and electrons in such hole-dominated matrix material.

Table 5. Characteristics of Stable *pin*-OLED Series **IV**−**VII** and **VIII**−**XII**

device	turn-on voltage [V]	driving voltage [V] at 1000 cd/m^2	lifetime t_{80} [h]	lifetime t_{50} [h]	η_P [lm/W] at 1000 cd/m^2
IV	1.8	3.7	1700	13500	4.5
V	1.8	3.5	57	512	4.7
VI	1.8	3.5	126	1050	3.9
VII	2.3	3.95	345	3500	3.5
VIII	1.9	4.2	4700	51000	3.4
IX	1.9	4.1	7200	58000	3.9
X	1.7	3.5	177	1400	4.3
XI	1.7	3.5	82	3500	3.8
XII	2.0	3.4	6	800	3.9

It can be easily seen that the operating lifetime is strongly correlated with the employed ancillary ligands. The devices based on [(fpmqx)$_2$Ir(pic)] (**V**) and [(fpmqx)$_2$Ir(acac)] (**VI**), with t_{50} lifetimes of 512 and 1050 h, underperform compared to the device (**VII**) using [Ir(piq)$_3$]. Unlike its counterparts, [(fpmqx)$_2$Ir(trz)] in device **IV** shows a superior operating lifetime compared to all other emitters. The extrapolated t_{50} lifetime of 13 500 h is about 4 times longer than that for device **VII**, using [Ir(piq)$_3$]. The luminance decrease at the beginning of the measurement is especially limited, which results in a high t_{80} lifetime of 1700 h. Because of these promising lifetime values, we tested a mixed matrix system of α-NPD and BAlq with the intention of creating a balanced charge transport and avoiding such strong localized degradation at the adjacent hole-blocking layer of BAlq. The ambipolar charge transport of a mixed α-NPD/BAlq layer has been demonstrated for the application in hybrid white OLEDs.[28] A mixed matrix host of BAlq and 15% α-NPD has also been used to optimize the charge carrier balance and therefore the efficiency in OLEDs using [Ir(piq)$_3$] as an emitter.[29] The effects of such a mixed matrix host on the device lifetime have not yet been presented in the literature.

The results for the mixed matrix devices are given in Figure 7b. Despite the limited difference in the resulting device efficiencies (Table 5) for mixed matrix OLEDs, all devices (**VIII**−**XII**) show enhanced operating lifetime performances, except for [Ir(piq)$_3$]. For instance, the power efficiencies for the devices **VIII** and **IX** are even lower than in device **IV**, where [(fpmqx)$_2$Ir(trz)] was doped into a neat α-NPD host. The mixed matrix concept is however clearly superior to the neat matrix as far as device lifetimes are concerned. These enhanced lifetimes can be ascribed to the delocalization of the recombination and emission zone. We expect the recombination zone to be broadened and

(27) Féry, C.; Racine, B.; Vaufrey, D.; Doyeux, H.; Cinà, S. *Appl. Phys. Lett.* **2005**, *87*, 213502.

(28) Schwartz, G.; Ke, T.-H.; Wu, C.-C.; Walzer, K.; Leo, K. *Appl. Phys. Lett.* **2008**, *93*, 073304.

(29) Deaton, J. C.; Place, D. W.; Brown, C. T.; Rajeswaran, M.; Kondakova, M. E. *Inorg. Chim. Acta* **2008**, *361*, 1020–1035.

more extended into the whole emission layer with an increasing amount of BAlq (up to a point where the recombination zone becomes strongly localized at the hole transport layer (α-NPD)). [Ir(piq)$_3$] in this case shows the worst performance, which we did not expect. We suppose that the [Ir(piq)$_3$] emitter works well in hole-dominated device setups but not in such mixed matrix systems or electron-dominated matrix materials.[7] The trends concerning the type of used ancillary ligands are also reflected in these data sets. Such a marked influence of the ancillary ligands on the operating stability of OLEDs has never been established before. We assume that the substantial differences in lifetimes can be explained by their stability toward charge carriers and excitons. The strongly electron-accepting character of the triazolylpyridine ligand might limit the electron stress for the quinoxaline ligands and act as an antenna or transporter. The devices **VIII** (ratio α-NPD/BAlq = 1:1) and **IX** (ratio α-NPD/BAlq = 1:3), using [(fpmqx)$_2$Ir(trz)] as a dopant, demonstrated an extrapolated operating lifetime of t_{50} = 51 000 and 58 000 h, respectively. Furthermore, the voltage increase over 1000 h amounted to 0.2 V for both **VIII** and **IX**.

Summary

We have synthesized and characterized a new series of orange−red-emitting iridium complexes bearing 2-(4-fluorophenyl)-3-methylquinoxaline cyclometalated ligands that are suitable for serving as commercial orange−red triplet emitters. All complexes can be easily prepared with high yields, and all are stable in the air. These complexes are easy to process as small molecules in ultra-high vacuum processes, which makes them good candidates for OLED applications. The complexes **1** and **2** have been additionally characterized by X-ray diffraction. Optical and electrochemical properties have been analyzed and compared with earlier reported "symmetric" 2,3-bis(4-fluorophenyl) quinoxaline iridium complexes. Because of the phosphorescent line shapes and low Stokes shifts, we propose that emission originates predominantly from a ^{3}MLCT state with a lesser admixture of totally ligand-based $^3(\pi-\pi^*)$ states. These complexes exhibit strong phosphorescence with emission quantum yields (Φ_p = 0.39−0.42) in toluene solution and short triplet lifetimes. Bright orange to red electroluminescent devices have been fabricated using new iridium complexes as emitters in simple test-device architectures. All devices showed high external quantum efficiencies in the range of 8−12% and a limited roll-off of efficiency values over a wide range of current densities.

The analysis of the operating lifetimes of the various stable device setups, using neat and mixed matrix concepts, can lead to a deeper understanding of OLED degradation and the role the emitters can play. We have realized stable OLEDs with a marked dependency on the nature of the ancillary ligands. By using [(fpmqx)$_2$Ir(trz)], OLEDs with superior long-time stability were realized.

Acknowledgment. The authors thank the Federal Ministry of Education and Research (BMBF) of Germany (CARO project; 01 BD 0687) for financial support.

Supporting Information Available: A crystallographic information file is available. This material is available free of charge via the Internet at http://pubs.acs.org.